


## Viscosity of capsule suspensions: Effects of internal-external viscosity ratio and capsule rupture release

Huiyong Feng,<sup>1,2</sup> Haibo Huang,<sup>2</sup> Jian Hou,<sup>3,4</sup> Chao Li,<sup>1</sup> and Bei Wei<sup>3,4</sup> 

<sup>1</sup>*Norinco Group Testing and Research Institute, Xi'an 710116, China*

<sup>2</sup>*Department of Modern Mechanics, University of Science and Technology of China, Hefei, Anhui 230026, People's Republic of China*

<sup>3</sup>*State Key Laboratory of Deep Oil and Gas, China University of Petroleum (East China), Qingdao 266580, People's Republic of China*

<sup>4</sup>*School of Petroleum Engineering, China University of Petroleum (East China), Qingdao 266580, People's Republic of China*



(Received 3 October 2023; accepted 27 August 2024; published 16 September 2024)

This work explores the variation of viscosity of capsule suspension during the process of capsule rupture and polymer release using the immersed-boundary lattice Boltzmann method. The variation of viscosity is classified into three stages in the rupture process: the deformation stage, the rupture stage, and the stable stage. In the process of polymer release, two new stages of the variation of viscosity emerge: the diffusion stage and the dilution stage. Furthermore, the influence of viscosity ratio ( $\lambda$ ) on the viscosity is investigated. We find that the effective viscosity grows with  $\lambda$  and approaches the solid particle limit for very large  $\lambda$ , reflecting a similar behavior in the capsule shape. Finally, an available law that relates suspension viscosity to  $\lambda$ , capillary number (Ca), and volume fraction ( $\phi$ ) is established. The findings of this research have potential applications in fields such as oil exploration and capsule transportation.

DOI: [10.1103/PhysRevFluids.9.093602](https://doi.org/10.1103/PhysRevFluids.9.093602)

### I. INTRODUCTION

In the field of oil development, polymer flooding is a popular method for enhancing oil recovery [1]. With the addition of polymers, the viscosity of the injected water is increased, while the oil-to-water viscosity ratio is reduced. This helps inhibit viscous fingering and improve the sweep coefficient, resulting in a significant improvement in oil recovery [2]. However, a higher injection rate is required when using polymer flooding in offshore oil fields and low-permeability fields [3,4]. On the one hand, the most commonly used polymers, for example, partially hydrolyzed polyacrylamide (HPAM), present the problem of shear degradation in the wellbore and near-well zone. Experimental studies have shown that the viscosity loss of a polymer due to shear degradation can reach 50–70% during the injection process [5,6]. On the other hand, as the injection pressure is proportional to the flow rate and fluid viscosity, the combined increase in viscosity (compared with water) and the flow rate leads to a higher injection pressure. This results in poor polymer injectivity because of facility constraints [7].

To address the issues of shear degradation and low injection efficiency, solutions have been proposed from both chemical and mechanical perspectives. One approach involves the use of associative polymers, which form supramolecular networks through the *in situ* assembly of high molecular weight polymers, thereby increasing the viscosity [8–10]. These associative polymers can be modified by adjusting the salinity and temperature. However, they remain susceptible to shear damage and exhibit significant retention in porous media. Another option is the utilization of biofilms instead of synthetic polymers. Biofilms are highly resistant to shearing but can be easily

degraded by bacterial infection [11,12]. Mechanical methods involve the implementation of flow control devices and innovative throttling geometries to minimize shear rates. However, the proposed solutions either fail to completely eliminate shear degradation or involve costly retrofitting [13,14].

In this research, the idea of encapsulating polymers by synthesizing micronano capsules has been proposed. This is similar to the approach used for medical enteric-coated capsules. This method ensures that the polymer is not released, while also providing strong shear resistance and good injectability. Once the capsule reaches its destination, it can rupture under specific conditions, such as a high temperature or pH, resulting in the release of the polymer and an increase in the viscosity [15–17]. However, during transportation, the capsules may rupture due to collisions and fluid shear, which can reduce transportation efficiency. Therefore, it is crucial to investigate the motion of polymer-encapsulated capsules and understand the factors that contribute to capsule rupture. In this study, we aim to investigate capsule rupture under different mechanical properties of the capsule membrane.

Previous studies have explored the rupture of capsules and the release of polymers. For instance, research on nonspherical polysiloxane microcapsules in a rotating device has shown that capsules tend to rupture first at their poles [18,19]. Coarse-grained molecular dynamics simulations conducted by Liu *et al.* have demonstrated that large vesicles can break up into smaller vesicles or fragments after rupturing [20]. Additionally, numerical simulations and experiments have been conducted to study the deformation and rupture of capsules in shear flows, revealing various morphologies after rupturing [21–23]. As for the encapsulation of polymers, previous studies have examined possible preparation methods [15–17]. However, there is currently no research available on encapsulating polymers and their subsequent release after capsule rupture.

The objective of this research is to investigate the transport and rupture processes of encapsulated polymer capsules through numerical simulations. The study is divided into three main parts: (i) an analysis of the rupture of the capsule and its impact on the flow properties of the suspension, (ii) an examination of the release of the polymer and its effect on the viscosity of the suspension, and (iii) an investigation of the effect of high  $\lambda$  on the viscosity of suspension. The article is structured as follows. In Sec. II, we provide a description of the problem and introduce the numerical method used. The results and discussion are presented in Sec. III. Finally, the conclusions are summarized in Sec. IV.

## II. PROBLEM STATEMENT AND METHODOLOGY

This study mainly investigated the effect of polymer encapsulated capsules on the viscosity of suspensions in shear flow. A circular capsule with radius  $a$  is placed in a computational with height  $h$ , see Fig. 1(a). The velocity of the wall is  $u$  and the shear rate  $\gamma$  is  $2u/h$ . In this study, length, velocity, and time are dimensionless by  $a$ ,  $a/\gamma$ , and  $1/\gamma$ , respectively.

### A. Membrane dynamics

The capsule is assumed to be formed by a coarsed-grained membrane (composed of hundreds of Lagrangian nodes) surrounding liquid and the membrane thickness is negligible. The elastic model is mainly composed of two elastic forces: tensile force and bending force, which can prevent excessive deformation and expansion of capsules. The tensile force  $T_e$  is parallel to the membrane surface:

$$T_e = k_s(\epsilon - 1), \quad (1)$$

where  $\epsilon$  is strain, and  $k_s$  is the shear modulus. The bending force  $T_b$  is perpendicular to the membrane surface and can be defined as

$$T_b = \frac{d}{dl}[k_b(\kappa - \kappa_0)], \quad (2)$$

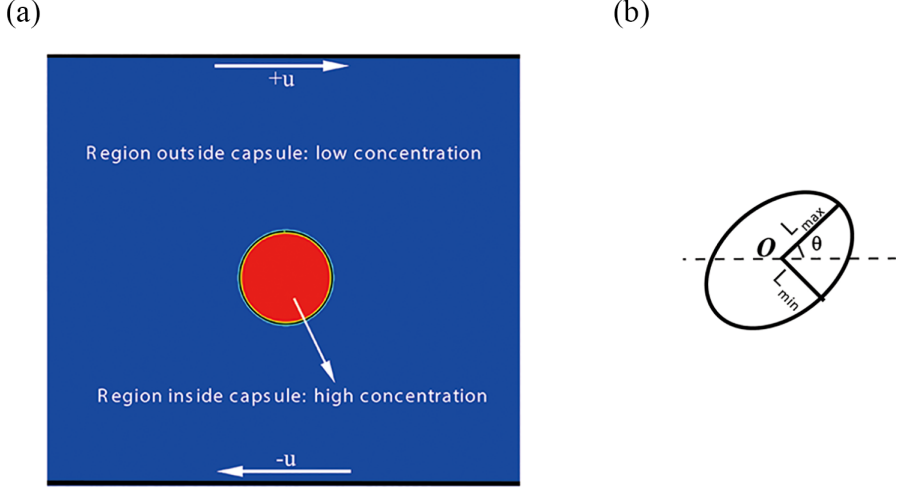


FIG. 1. (a) The diagram of a capsule and the initial distribution of the polymer in a shear flow. Red region: the high-concentration region inside the capsule. Blue region: the low-concentration region outside the capsule. (b) The deformation of the capsule under fluid shear.  $O$  represents the center of the capsule.  $L_{\max}$  and  $L_{\min}$  denote the lengths of the long and short axes of the capsule.  $\theta$  indicates the inclination angle of the capsule. The dashed line represents the horizontal line.

where  $\kappa$  and  $\kappa_0$  are the instantaneous and initial curvature, respectively.  $k_b$  is the bending modulus. The total elastic force  $\mathbf{T}$  is the sum of tensile force and bending force:

$$\mathbf{T} = T_t \mathbf{t} + T_b \mathbf{n}, \quad (3)$$

where  $\mathbf{t}$  is the tangential unit vector, and  $\mathbf{n}$  is the normal unit vector.

### B. Numerical method

The lattice Boltzmann method (LBM) is used to simulate the fluid flow in the entire domain. Macroscopically, it is able to solve the incompressible Navier-Stokes equations. The lattice Boltzmann equation is

$$f_i(\mathbf{x} + \mathbf{e}_i \Delta t, t + \Delta t) - f_i(\mathbf{x}, t) = -\frac{\Delta t}{\tau} (f_i(\mathbf{x}, t) - f_i^{eq}(\mathbf{x}, t)) + \Delta t F_i, \quad (4)$$

with

$$f_i^{eq}(\mathbf{x}, t) = \omega_i \rho \left[ 1 + \frac{\mathbf{e}_i \cdot \mathbf{u}}{c_s^2} + \frac{(\mathbf{e}_i \cdot \mathbf{u})^2}{2c_s^4} - \frac{\mathbf{u}^2}{2c_s^2} \right], \quad (5)$$

where  $f_i(\mathbf{x}, t)$  is the discretized distribution function at location  $\mathbf{x}$  and time  $t$ ,  $f_i^{eq}(\mathbf{x}, t)$  is the equilibrium distribution function,  $\mathbf{e}_i$  is the discretized velocity vector, and the  $D_2Q_9$  velocity model is adopted.  $\omega_i$  is the weighting factor.  $\omega_i = 4/9$  for  $i = 0$ ;  $\omega_i = 1/9$  for  $i = 1, 2, 3, 4$ ; and  $\omega_i = 1/36$  for  $i = 5, 6, 7, 8$ .  $c_s = \frac{1}{\sqrt{3}} \frac{\Delta x}{\Delta t}$  is the lattice sound speed, where  $\Delta x$  and  $\Delta t$  are the grid length and time step, respectively.  $\tau$  is the relaxation time.  $F_i$  is a source term accounting for external force and will be used here to incorporate the forces exerted by the membrane on the fluid through the immersed boundary method (IBM).

The macroscopic quantities can be obtained from the moments of the distribution function:

$$\rho = \sum f_i \quad (6)$$

and

$$\mathbf{u} = \sum f_i \mathbf{e}_i / \rho \quad (7)$$

The immersed boundary method (IBM) is used for the fluid-membrane coupling. In the IBM, the Lagrangian nodes of capsules are interacting with the Eulerian fluid nodes using an interpolation function in a two-way coupling scheme: the velocity of a Lagrangian point is interpolated from the surrounding fluid nodes, i.e.,

$$\mathbf{u}(\mathbf{s}) = \sum_f \delta(\mathbf{s} - \mathbf{x}) \mathbf{u}(\mathbf{x}), \quad (8)$$

where  $\mathbf{s}$  and  $\mathbf{x}$  are the locations of the Lagrangian points and fluid nodes, respectively.  $\delta$  is the interpolation function. The location of each Lagrangian point and the new geometry of the capsule at the next time step can be determined from the kinematic formula. The force obtained from the constitutive equation should be spread to surrounding fluid nodes, i.e.,

$$\mathbf{F}(\mathbf{x}) = \sum_f \delta(\mathbf{s} - \mathbf{x}) \mathbf{T}(\mathbf{s}). \quad (9)$$

It is noted that this force should be added to the lattice Boltzmann equation as an external force. The interpolation function is chosen to be

$$\delta(\mathbf{s} - \mathbf{x}) = \delta(x - x(\mathbf{s})) \delta(y - y(\mathbf{s})), \quad (10)$$

where

$$\delta(r) = \begin{cases} \frac{1}{4} (1 + \cos(\frac{\pi|r|}{2})), & |r| \leq 2 \\ 0, & |r| > 2. \end{cases} \quad (11)$$

The IB-LBM is mature and widely adopted in the field of fluid-solid interaction, especially in the simulation of capsule suspension. For a comprehensive understanding and validation, we recommend referring to our previous studies [24–26].

For the polymer, we only consider the viscosity and concentration but not the chemical properties. The diffusion of polymer is simplified to a typical convective diffusion scenario. Hence, the diffusion behavior of the polymers can be described using the convection-diffusion equation. The general form of the convection-diffusion equation is as follows:

$$\frac{\partial C}{\partial t} + \vec{u} \cdot \nabla C = D \nabla^2 C, \quad (12)$$

where  $C$  is the concentration of the polymer and  $D$  is the diffusion coefficient. Both parameters are all converted to the LB field and  $D = 0.001$  in this study. The fluid velocities are obtained after solving the LBM equation. The concentration convection-diffusion equation is mainly solved using the finite difference method.

### C. Key parameters and observables

Five main dimensionless parameters are included in the numerical simulation: the Reynolds number  $Re = 4\rho\gamma a^2/\mu$ , which is set as 0.1 such that the inertia can be neglected. The capillary number  $Ca = \mu\gamma a/k_s$ , which is associated with the elasticity of the capsule. The dimensionless bending modulus  $E_b = k_b/(a^2 k_s)$ , and the viscosity ratio  $\lambda = \frac{\mu_{in}}{\mu_{out}}$ , which is used to describe the polymer concentration or viscosity inside the capsule.  $\mu_{in}$  and  $\mu_{out}$  are the fluid viscosity values inside and outside the capsule. The volume fraction of capsules,  $\phi = N_p \pi a^2/h^2$  where  $N_p$  is the number of capsules.

The Taylor deformation parameter  $D_{xy} = \frac{L_{\max} - L_{\min}}{L_{\max} + L_{\min}}$  is usually used to quantify the deformation of capsules. Figure 1(b) shows the deformation of a capsule in a simple shear flow. Generally speaking, a large  $D_{xy}$  denotes large deformation.

Suspension viscosity  $\mu_a$  is another important parameter in this study. It can be calculated from the wall stress in simple shear flows [27,28]

$$\mu_a = \frac{\mu}{\mu_0} = \frac{\langle \sigma \rangle}{\rho v \gamma}, \quad (13)$$

where  $\mu$  is the effective viscosity, and  $\mu_0$  is the viscosity of suspension where the concentration of polymer is 0.  $\langle \rangle$  represents the statistical average in time and  $\sigma$  is the average shear stress on the wall:

$$\sigma = \rho v (\partial_y w + \partial_x v) = - \left( 1 - \frac{1}{2} \tau \right) \sum f_i^{\text{neq}} e_{iy} e_{ix}, \quad (14)$$

where  $f_i^{\text{neq}} = f_i - f_i^{\text{eq}}$  is the nonequilibrium distribution function,  $f_i$  is the distribution function, and  $f_i^{\text{eq}}$  is the equilibrium distribution function.  $e_{iy}$  and  $e_{ix}$  are the unit vectors of the lattice velocity. The quantities involved in the above calculations are all from LBM, which can be referred to Refs. [27,28]. The intrinsic viscosity of suspension is defined as

$$[\mu] = \frac{\mu_a - 1}{\phi}. \quad (15)$$

### III. RESULTS AND DISCUSSION

In the following subsections, we mainly investigate the influence of rupture of capsules and release of polymers on the viscosity of suspension. What's more, the effect of concentration of polymers as well as the  $\lambda$  on the flow properties is then analyzed.

#### A. Effect of capsule rupture

When the strain of the capsule exceeds a strain limit, the capsule ruptures. Therefore, a simplified capsule rupture condition is when the distance between two Lagrangian points on the capsule membrane exceeds a specific threshold, the stress between the two points disappears, that is, rupture occurs. The length threshold of adjacent Lagrangian points is 20%, which is the same as the setting adopted by Rahmat *et al.* [21].

Figure 2 shows the deformation and rupture of a capsule at different times. As time progresses, the deformation of the capsule increases gradually, from the initial round shape to an oval shape, as shown in Figs. 2(a)–2(c). When the capsule is stretched to a certain extent, the capsule first ruptures on the short axis where the stress is the largest, as seen in Fig. 2(d). The capsule then breaks up into two parts, as seen in Figs. 2(e) and 2(f). Our results are similar to those found in previous simulations and experiments [21–23], and the rupture criterium is set accurately.

Figure 3 quantitatively demonstrates the deformation and inclination of a capsule with and without rupture. The dashed line represents the cases where the rupture model is not added. It can be seen that  $D_{xy}$  increases first and then stabilizes to a constant value, that is, the capsule reaches a steady state. When the rupture model is added (see the solid line), the deformation is the same as that without the rupture model when  $t < t_0$ . At  $t = t_0$ , the capsule ruptures and then forms two small segments. The two segments gradually move apart, so  $D_{xy}$  keeps increasing with time. In the same way, the inclination angle  $\theta$  of the capsule reaches a stable value in the absence of the rupture model and the inclination angle continues to decrease when the rupture model is added.

We also conduct a mesh convergence verification for the capsule rupture process. We select three grid lengths  $\Delta x = 0.05, 0.04, 0.02$ , where  $\Delta x$  is the unit mesh length. The distance between two Lagrangian points is the same as or slightly smaller than the grid lengths, so the numbers of Lagrangian points corresponding to the above three grid lengths were 160, 200, and 320,

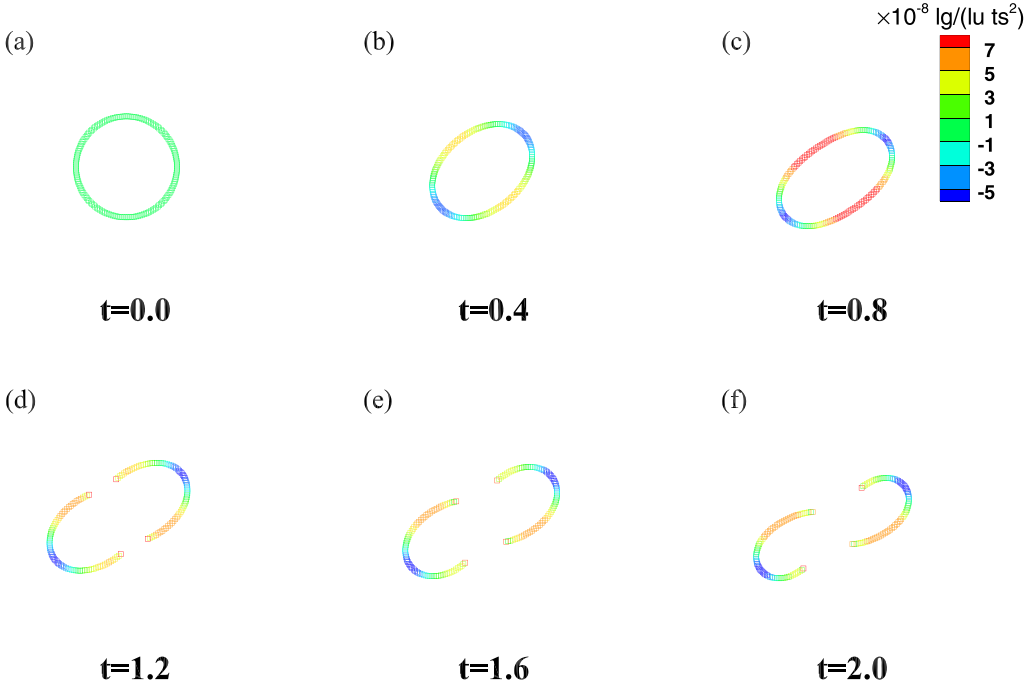


FIG. 2. The shape and rupture of capsules at different times. The color represents the tensile stress of the capsules, where  $lg$  and  $lu$  is the unit of mass and length in LB field. Parameter setting:  $Re = 0.1$ ,  $Ca = 0.1$ ,  $E_b = 0.05$ .

respectively. It can be seen from Fig. 3 that the capsule deformations and inclination angles are the same for the three grid lengths, no matter whether the capsule ruptures or not. It is noted that  $D_{xy}$  and  $\theta$  do not have any physical meaning after the rupture of capsules. The solid lines of  $t > t_0$  in Fig. 3 are only used to distinguish whether the capsule has ruptured. In subsequent calculations, the grid length of the fluid is set to 0.04 and the number of Lagrangian points is set to 200.

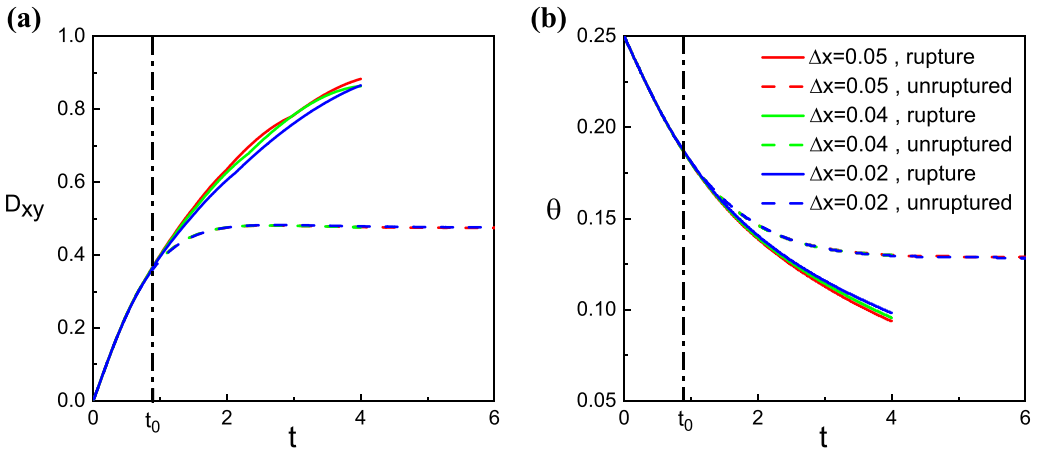


FIG. 3. (a)  $D_{xy}$  and (b)  $\theta$  as a function of time under different mesh densities. The solid and dashed lines represent the conditions of the capsules with and without rupture models and  $t_0$  represents the initial rupture time.  $Ca = 0.1$ ,  $h = 10a$ ,  $E_b = 0.05$ ,  $\lambda = 1$ . The capsules do not include the polymer.

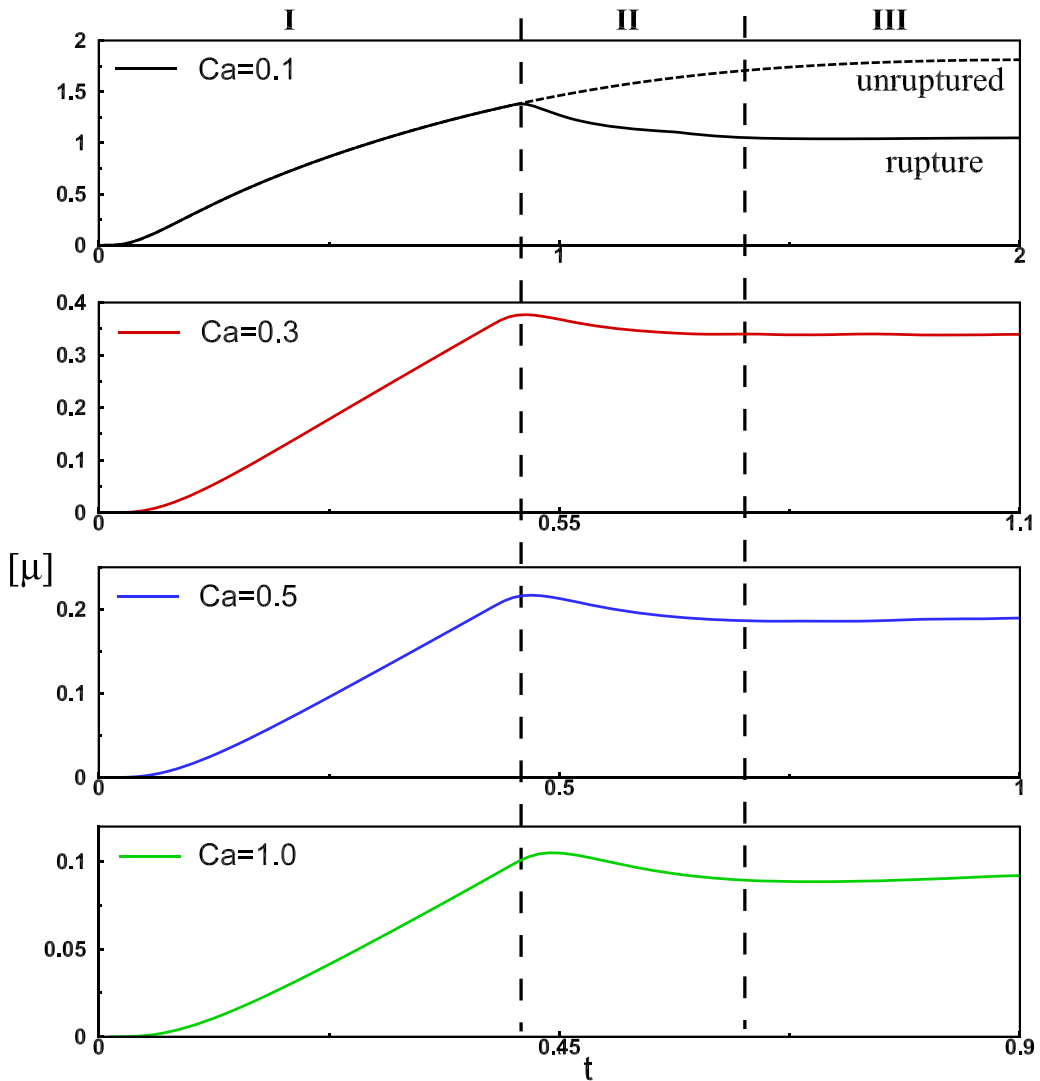


FIG. 4.  $[\mu]$  as a function of time during the rupture of the capsule.  $h = 10a$ ,  $E_b = 0.05$ ,  $\lambda = 1$ . The dashed line is the variation of  $[\mu]$  without capsule rupture. The vertical dotted lines are the dividing lines between stages.

The complex mechanisms and numerical simulations of capsule rupture have not yet been fully explored, which limits our ability to provide quantitative verifications. Therefore, we adopted a relatively simple and previously used rupture criterion, followed by grid convergence verification. This criterion, being straightforward, easy to understand, and consistent with physical laws, serves our purpose effectively. On the other hand, the primary focus of our research is the variation in viscosity before and after capsule rupture. The rupture process itself is merely an intermediate stage. The rupture criterion is set to facilitate polymer release, and its impact on the viscosity changes before and after rupture is minimal. Therefore, while a more detailed quantitative comparison would enhance the rigor, it does not significantly affect the main findings related to viscosity changes.

The effect of capsule rupture on the intrinsic viscosity  $[\mu]$  is first investigated. Figure 4 shows the change of  $[\mu]$  with time when the capsule rupture model is added. It can be seen that the changes of  $[\mu]$  under different  $Ca$  are the same, and can be divided into three stages. Stage I is the deformation

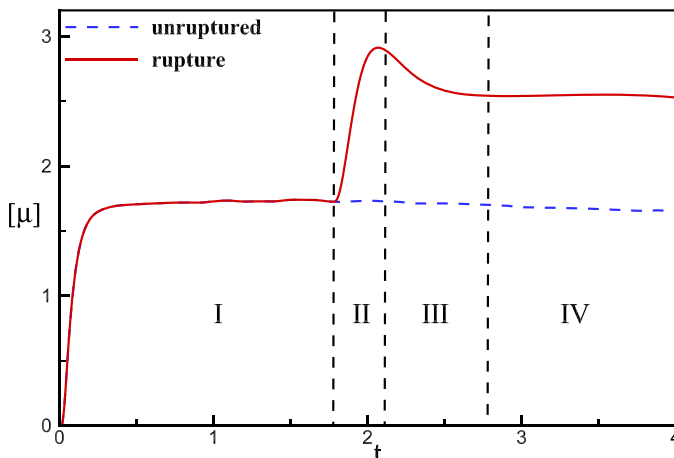


FIG. 5.  $[\mu]$  as a function of time at  $\lambda = 10$ . The red dashed and solid blue lines represent the cases with and without capsule rupture, respectively. The dotted lines are the dividing lines between stages. The parameter settings are  $Re = 0.1$ ,  $Ca = 0.5$ .

stage. The capsule has not yet ruptured, the deformation of the capsule increases with time, and  $[\mu]$  also gradually increases. Stage II is the rupture stage. The deformation reaches the threshold and the capsule begins to rupture. After the capsule ruptures, the stress of capsule decreases (see Fig. 2) and the effect of the capsule on the fluid is weakened. Due to this reason,  $[\mu]$  decreases and becomes lower than that when the capsule is not ruptured, see the dashed line at  $Ca = 0.1$ . Stage III is called the stable stage. The rupture of the capsule is complete. The effect of the broken part on the fluid does not change and  $[\mu]$  does not change. The viscosity of suspension at stable stage is lower than the viscosity of suspension when the capsule is not ruptured.

When the polymer is contained inside the capsules, the rupture of the capsules is often accompanied by the release and diffusion of the polymer. In the next section, we mainly investigate the effect of the release of polymer on  $[\mu]$  of suspension. The concentration or viscosity of the polymer inside the capsule can be measured through the viscosity ratio  $\lambda$ . The larger  $\lambda$ , the higher the polymer concentration. The viscosity of the polymer suspension is closely related to the concentration and can be described by a viscosity-concentration curve. The polymer studied in this paper is hydrolyzed polyacrylamide (HPAM), whose viscosity concentration curve conforms to the following exponential relationship:  $\mu = \mu_0 e^{0.88C}$ .

After the capsules rupture, the polymer diffuses with the fluid into the surrounding medium. Figure 5 shows the change in  $[\mu]$  during the rupture of a capsule containing polymer. It can be seen that the viscosity change process of the suspension can be divided into four stages. Stage I [Fig. 6(a)] is the deformation stage. The capsule is not ruptured, the deformation increases with time, and  $[\mu]$  increases. Stage II [Fig. 6(b)] is the diffusion stage. The capsule ruptures and the polymer diffuses to the outside of the capsule. The polymer concentration in the suspension surrounding the capsules increases, resulting in an increase in  $[\mu]$ . Stage III [Fig. 6(c)] is the dilution stage. The polymer is completely released into the surrounding fluid. At this stage, the effect of the rupture begins to manifest. The effect of the capsule on the fluid is weakened and the viscosity of the suspension is reduced. Stage IV [Fig. 6(d)] is the stable stage. The effects of the polymer diffusion and capsule rupture disappear and  $\mu_a$  stabilizes. Unlike in the rupture of capsules that do not contain polymers, the viscosity change has a regrowth stage (Stage II) due to polymer diffusion. The diffusion stage is the main stage that causes the viscosity growth of capsule suspension.



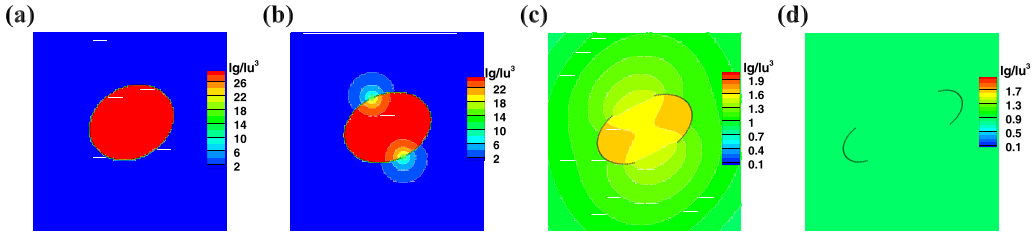


FIG. 6. The forms of the capsule and the contour of the concentration after the rupture at  $Re = 0.1$ ,  $Ca = 0.5$ ,  $\lambda = 20$ . (a)–(d) correspond to the four regimes of viscosity change. The color represents the concentration of the polymer. When the color is close to red, the concentration is high. When the color approaches blue, the concentration is low.

### B. Effect of $\lambda$ on $\mu_a$

During the actual polymer injection process, in order to protect the polymer and reduce viscosity loss, the capsule should not rupture before being transported to its destination. Therefore, in this section, we focus on the impact of  $\lambda$  on  $\mu_a$  when the capsules are not ruptured. Figure 7 shows the structures of capsules under different  $\lambda$  in equilibrium state. It can be seen that the deformation of the capsule becomes smaller as  $\lambda$  increases. In the case of high  $\lambda$ , such as  $\lambda = 100$ , the capsules

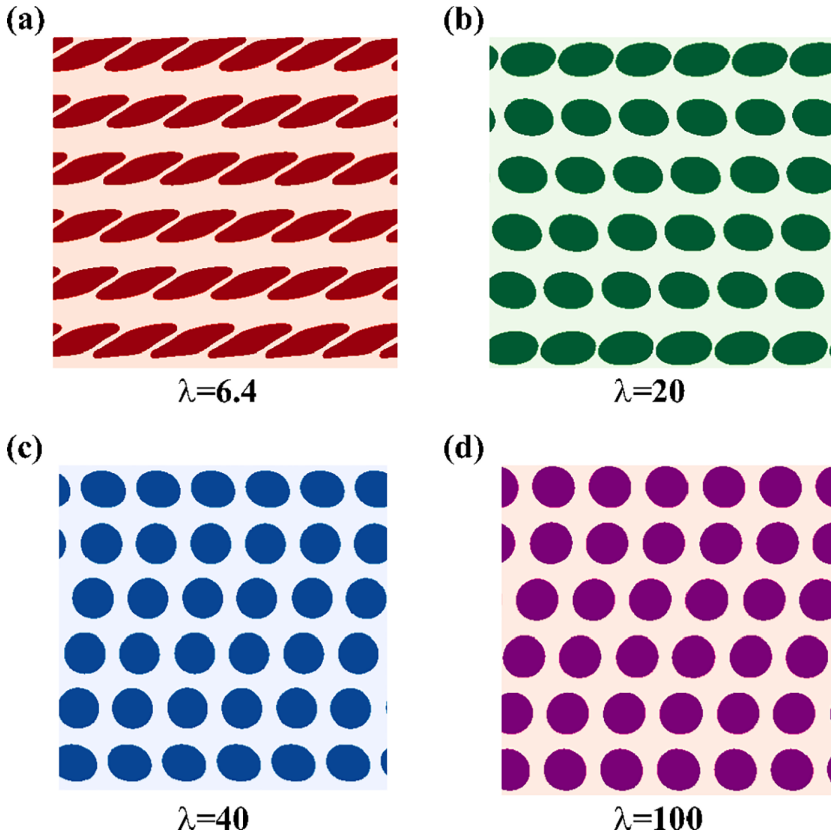


FIG. 7. The stable forms of capsules under different  $\lambda$  at  $Re = 0.1$ ,  $Ca = 0.5$ ,  $E_b = 0.05$ ,  $\phi = 44.18\%$ . (a)  $\lambda = 6.4$ , (b)  $\lambda = 20$ , (c)  $\lambda = 40$ , (d)  $\lambda = 100$ .

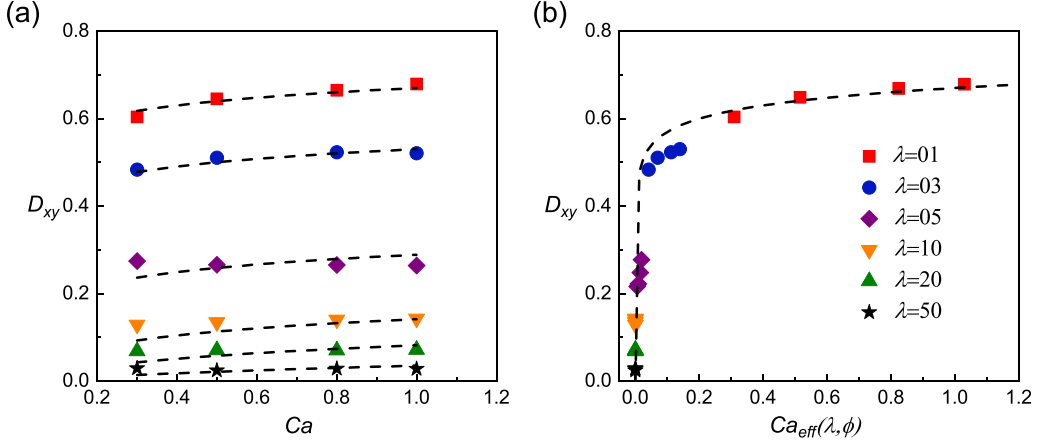


FIG. 8. (a)  $D_{xy}$  as a function of  $Ca$  at different  $\lambda$ . (b) The change in  $D_{xy}$  with redefined  $Ca_{\text{eff}}$ . The dashed line represents the curve fitted through Eqs. (11) and (12).

hardly deform. This is the same effect as that of a large shear modulus (small  $Ca$ ). Aouane *et al.* studied the universal law of  $\mu_a$  as a function of  $Ca$ ,  $\phi$ , and the bulk modulus  $C$  [29].  $\lambda$  is also an important factor that affects the morphology of capsules.

Figure 8(a) shows the change in  $D_{xy}$  under different  $Ca$  and  $\lambda$ .  $D_{xy}$  shows a similar variation trend with  $Ca$  under different  $\lambda$ . Aouane *et al.* points out that the change in  $D_{xy}$  with  $Ca$  satisfies the log function [29]:

$$D_{xy} = D(Ca, \phi, \lambda) = Ag\left(\frac{Ca}{Ca^*(\phi, \lambda)}\right), \quad (16)$$

where  $A$  is a constant and  $Ca^*$  is a function of  $\phi$  and  $\lambda$ . From data fitting, we can determine that  $A = 0.1$ . Values of  $\lambda = 1, 5, 10, 20$ , and  $50$  correspond to  $Ca^* = 2.0 \times 10^{-7}, 1.3 \times 10^{-3}, 4.0 \times 10^{-2}, 1.8 \times 10^{-1}$ , and  $8.0 \times 10^{-1}$ , respectively.

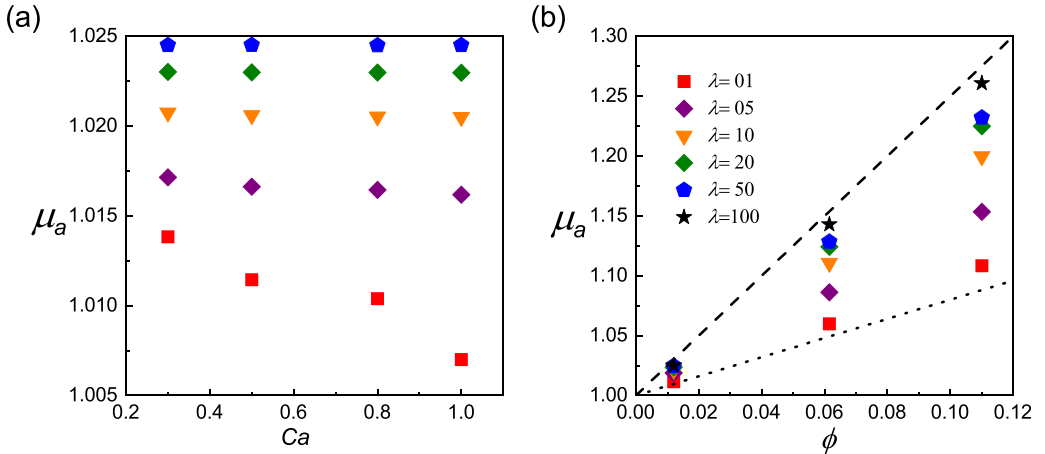


FIG. 9. (a)  $\mu_a$  as a function of  $Ca$  at different  $\lambda$ . (b)  $\mu_a$  as a function of  $\phi$ . The slope of the long dashed line is 2.5, and the line represents Einstein's viscosity formula  $\mu_a = 1 + 2.5\phi$ , that is, the  $\mu_a$  of a dilute solution of rigid particles. The slope of the short dotted line is 0.8.

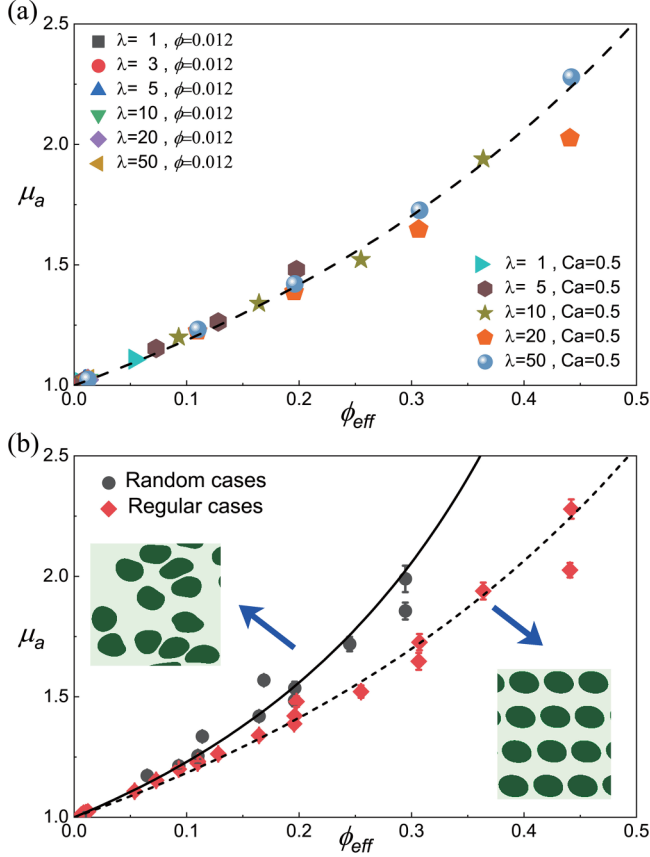


FIG. 10. (a)  $\mu_a$  as function of the redefined volume fraction  $\phi_{\text{eff}}$ . The dashed line is drawn according to Eq. (18). (b) Comparison of viscosity when capsules are in random or regularly arranged state in equilibrium state, the solid line is a simple fitting of circular dots. The two small images inserted in (b) represent the typical forms of random and regular cases, respectively.

When  $\lambda = 1$ ,  $\text{Ca} = \mu\gamma a/k_s$ . Through the self-similarity of the formula, we can redefine  $\text{Ca}$  to include information on  $\lambda$ . We replace  $k_s$  with  $e^{-\lambda+1}k_s$ . Therefore, the redefined  $\text{Ca}$  ( $\text{Ca}_{\text{eff}}$ ) is

$$\text{Ca}_{\text{eff}} = \frac{\mu\gamma a}{e^{-\lambda+1}k_s}, \quad (17)$$

Figure 8(b) shows a plot of  $D_{xy}$  and  $\text{Ca}_{\text{eff}}$ . It can be seen that the data points for different  $\lambda$  all fall on the same line. Therefore, the above redefinition of  $\text{Ca}$  is valid.

Now we consider the rheology of suspension. Figure 9(a) shows  $\mu_a$  as a function of  $\text{Ca}$  and  $\lambda$ . It can be seen that the larger  $\lambda$  is, the greater  $\mu_a$  is. When  $\lambda$  increases to a certain extent, for example, when  $\lambda = 50$ , for  $\text{Ca} = 0.3, 0.5, 0.8, 1.0$ ,  $\mu_a$  is about 1.025 and does not change [see the blue pentagons in Fig. 9(a)]. When  $\lambda$  is relatively small,  $\mu_a$  decreases with  $\text{Ca}$  [see the red squares in Fig. 9(a)]. Figure 9(b) shows the variation of  $\mu_a$  with  $\phi$  at different  $\lambda$ . It can be seen that with an increase in  $\lambda$ ,  $\mu_a$  as a function of  $\phi$  gradually approaches that of rigid particle suspension. When  $\lambda = 100$ , the change in  $\mu_a$  is nearly the same as that of a solution of rigid particles.

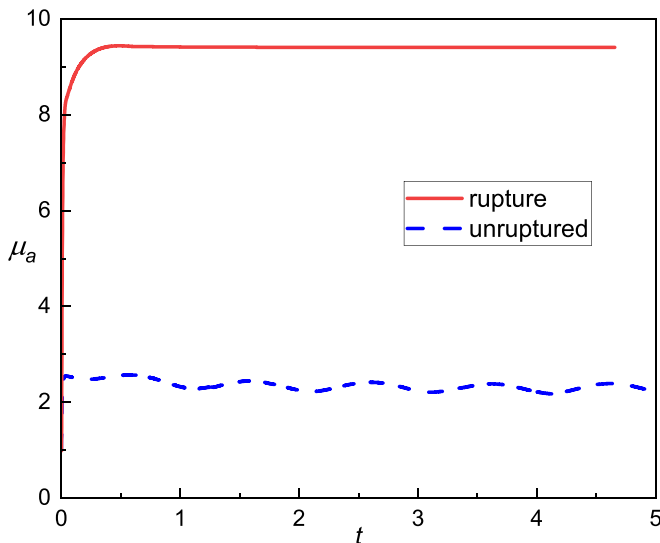


FIG. 11.  $\mu_a$  as a function of time when the capsules rupture and do not rupture at  $\phi = 44.18$ ,  $\lambda = 100$ . The red and blue lines represent the cases with and without rupture, respectively.

According to the formula by Eilers [30],  $\mu_a$  can be expressed as

$$\mu_a(\phi_{\text{eff}}) = \left[ 1 + \frac{B\phi_{\text{eff}}}{1 - \frac{\phi_{\text{eff}}}{\phi_m}} \right]^2, \quad (18)$$

where  $B$  is constant coefficient and  $\phi_m$  is the maximum packing fraction.  $\phi_{\text{eff}}$  is

$$\phi_{\text{eff}} = \frac{1 - D}{1 + D} \left( \frac{1 + b^2}{1 + \left(\frac{1-D^2}{1+D^2}\right)^2 b^2} \right)^{3/2} \phi, \quad (19)$$

where  $D = D_{xy}$  and is given by Eq. (16).

Next, we substitute the data in Figs. 9(a) and 9(b) into  $\phi_{\text{eff}}$  as defined by Eq. (19), take  $\phi_{\text{eff}}$  as the abscissa, organize the data for different  $\phi$ , and redraw the curve in Fig. 10(a). It can be seen that all the data are normalized on the same curve, which conforms to Eq. (18). When the structures of capsules are random in equilibrium state,  $\mu_a$  is slightly higher than that of the regular array, see Fig. 10(b). This can be understood since capsules in a random arrangement move more irregularly and have a greater impact on the flow field, resulting in higher viscosity. The variation in viscosity for both cases is consistent when  $\phi_{\text{eff}}$  is low. As  $\phi_{\text{eff}}$  increases, a slight difference between the two cases emerges, with the viscosity of the randomly arranged capsules being higher than that of the regular array. The chaotic arrangement of capsules lacks obvious patterns, making it challenging to summarize effective rules. This phenomenon warrants further exploration in future studies.

So far, based on previous work, we have preliminarily included  $\lambda$  in the formula of  $\mu_a$  to obtain the universal  $\mu_a - \phi_{\text{eff}}(\text{Ca}, \lambda, \phi)$  relationship. This may be helpful for predicting the viscosity of capsule suspension.

Finally, we compare the viscosities of the suspension with and without capsule rupture at high  $\lambda$ . From Fig. 5, we can see that the capsule does have a viscosifying effect after rupture, and the increase in the viscosity is less than 10% when  $\lambda$  and  $\phi$  are small. We then increase the  $\lambda$  and  $\phi$  of the capsule suspension [as shown in Fig. 7(d)]. Figure 11 shows that, after imposing these settings, if

the capsules do not rupture,  $\mu_a$  is about twice that of a pure solution. If the capsule ruptures,  $\mu_a$  rises rapidly to about ten times the value of the original solution, which meets experimental requirements [14,31]. The final  $\mu_a$  depends on  $\lambda$ . The greater  $\lambda$ , the greater  $\mu_a$  after the rupture of the capsule. The idea of encapsulating the polymers by synthesizing micronano capsules is an effective way to transport the polymer. So far, we have successfully numerically modeled the rupture of the capsule and the release of the polymer.

#### IV. CONCLUSION

In this research, the variation of viscosity of capsule suspension during the process of capsule rupture was first studied. During the process of the rupture of capsules, the variation of viscosity can be classified into three stages: the deformation stage, the dilution stage, and the stable stage. Then the model of polymer release was established through the concentration convection-diffusion equation. The diffusion process of the polymer and the change in viscosity after the rupture of the capsule was studied. Depending on the variation of viscosity, there are four stages: the deformation stage, the diffusion stage, the dilution stage, and the stabilization stage. After the capsule ruptures, the diffusion of the polymer can rapidly increase viscosity.

The effect of  $\lambda$  on the rheological properties of the suspension was also investigated without the rupture of the capsule. It is found that when  $\lambda$  is large enough ( $>100$ ), the variation trend of viscosity approaches that of a rigid particle suspension. Through redefining the shear modulus  $k_s$  and  $\phi_{\text{eff}}$ , which depends on  $\lambda$ ,  $Ca$ , and  $\phi$ , all viscosity data can be normalized on the same curve, which conforms to the previous viscosity formula. Finally, we compared the viscosity of the suspension with and without the rupture of capsules at high  $\lambda$ . This work can guide related work in capsule transportation, oil exploration, and other industrial fields.

#### ACKNOWLEDGMENTS

This work was supported by the Joint Funds of the National Natural Science Foundation of China (Grant No. U21B2070). The project was also supported by the Natural Science Foundation of China (NSFC), Grants No. 11772326 and No. 52374061. In addition, this research was supported by the Supercomputing Center of the USTC.

- 
- [1] R. Seright and D. Wang, Polymer flooding: Current status and future directions, *Pet. Sci.* **20**, 910 (2023).
  - [2] H. S. Rabbani, D. Or, Y. Liu, C.-Y. Lai, N. B. Lu, S. S. Datta, H. A. Stone, and N. Shokri, Suppressing viscous fingering in structured porous media, *Proc. Natl. Acad. Sci. USA* **115**, 4833 (2018).
  - [3] G. Flavien, R. Christophe, L. Lionel, and T. Antoine, Offshore polymer EOR injection philosophies, constrains and solutions, in *SPE Improved Oil Recovery Conference* (OnePetro, USA, 2020), Paper No. SPE-200368-MS.
  - [4] J. J. Sheng, B. Leonhardt, and N. Azri, Status of polymer-flooding technology, *J. Can. Pet. Technol.* **54**, 116 (2015).
  - [5] X. Xin, G. Yu, Z. Chen, K. Wu, X. Dong, and Z. Zhu, Effect of polymer degradation on polymer flooding in heterogeneous reservoirs, *Polymers* **10**, 857 (2018).
  - [6] A. M. Mansour, R. S. Al-Maamari, A. S. Al-Hashmi, A. Zaitoun, and H. Al-Sharji, In-situ rheology and mechanical degradation of EOR polyacrylamide solutions under moderate shear rates, *J. Pet. Sci. Eng.* **115**, 57 (2014).
  - [7] V. Torrealba and H. Hoteit, Improved polymer flooding injectivity and displacement by considering compositionally-tuned slugs, *J. Pet. Sci. Eng.* **178**, 14 (2019).
  - [8] A. Thomas, N. Gaillard, C. Favero, J. Bai, K. Green, and F. Wassmuth, Performance of associative polymers in porous media, in *IOR 2013-17th European Symposium on Improved Oil Recovery, St. Petersburg, Russia* (EAGE Publications BV, Houten, Netherlands, 2013).

- [9] R. S. Seright, T. Fan, K. Wavrik, H. Wan, N. Gaillard, and C. Favéro, Rheology of a new sulfonic associative polymer in porous media, *SPE Reservoir Eval. Eng.* **14**, 726 (2011).
- [10] D. Wever, F. Picchioni, and A. Broekhuis, Polymers for enhanced oil recovery: A paradigm for structure–property relationship in aqueous solution, *Prog. Polym. Sci.* **36**, 1558 (2011).
- [11] S. J. Geetha, I. M. Banat, and S. J. Joshi, Biotechnology in petroleum recovery: The microbial EOR, *Prog. Energy Comb. Sci.* **34**, 714 (2008).
- [12] M. Sveistrup, F. van Mastrigt, J. Norrman, F. Picchioni, and K. Paso, Viability of biopolymers for enhanced oil recovery, *J. Dispersion Sci. Technol.* **37**, 1160 (2016).
- [13] A. S. Monteiro and S. Da S. Fabrício, Test results of a comparison between a conventional and low shear valve and its effect on water/oil separation, in *Offshore Technology Conference Brasil, Rio de Janeiro, Brazil* (OnePetro, USA, 2019), Paper No. OTC-29949-MS.
- [14] B. Rashid, J. Stapley, P. Clifford, D. Chappell, M. Kiani, W. J. Andrews, and E. C. Hart, Successful field trial of a novel, reservoir-triggered polymer: Results, interpretation and simulation, in *SPE Improved Oil Recovery Conference, Tulsa, Oklahoma, USA* (OnePetro, USA, 2018), Paper No. SPE-190159-MS.
- [15] X. Lu, J. S. Katz, A. K. Schmitt, and J. S. Moore, A robust oil-in-oil emulsion for the nonaqueous encapsulation of hydrophilic payloads, *J. Am. Chem. Soc.* **140**, 3619 (2018).
- [16] H. Huang, T. Belwal, H. Aalim, L. Li, X. Lin, S. Liu, C. Ma, Q. Li, Y. Zou, and Z. Luo, Protein-polysaccharide complex coated W/O/W emulsion as secondary microcapsule for hydrophilic arbutin and hydrophobic coumaric acid, *Food Chem.* **300**, 125171 (2019).
- [17] A. Lavrenova, J. Farkas, C. Weder, and Y. C. Simon, Visualization of polymer deformation using microcapsules filled with charge-transfer complex precursors, *ACS Appl. Mater. Interfaces* **7**, 21828 (2015).
- [18] K.-S. Chang and W. L. Olbricht, Experimental studies of the deformation and breakup of a synthetic capsule in steady and unsteady simple shear flow, *J. Fluid Mech.* **250**, 609 (1993).
- [19] M. Husmann, H. Rehage, E. Dhenin, and D. Barthès-Biesel, Deformation and bursting of nonspherical polysiloxane microcapsules in a spinning-drop apparatus, *J. Colloid Interface Sci.* **282**, 109 (2005).
- [20] P. Liu, J. Li, and Y.-W. Zhang, Breakup of spherical vesicles caused by spontaneous curvature change, *Acta Mech. Sin.* **28**, 1545 (2012).
- [21] A. Rahmat, M. Barigou, and A. Alexiadis, Deformation and rupture of compound cells under shear: A discrete multiphysics study, *Phys. Fluids* **31**, 051903 (2019).
- [22] S. Joung, M. Song, and D. Kim, Synthetic capsule breakup in simple shear flow, *Phys. Fluids* **32**, 113603 (2020).
- [23] R. Chachanidze, K. Xie, J. Lyu, M. Jaeger, and M. Leonetti, Breakups of Chitosan microcapsules in extensional flow, *J. Colloid Interface Sci.* **629**, 445 (2023).
- [24] H. Feng, H. Huang, and X.-Y. Lu, Rheology of capsule suspensions in plane Poiseuille flows, *Phys. Fluids* **33**, 013302 (2021).
- [25] R. Cao, H. Feng, J. Hou, B. Wei, and H. Huang, Dynamic modes of a capsule under oscillating shear flow with finite inertia, *Phys. Fluids* **34**, 103324 (2022).
- [26] H. Feng, J. Zheng, B. Wei, J. Hou, and H. Huang, Capsule distributions and flow properties in curved tubes, *Phys. Rev. Fluids* **8**, 013604 (2023).
- [27] D. Qi and L. S. Luo, Rotational and orientational behaviour of three-dimensional spheroidal particles in Couette flows, *J. Fluid Mech.* **477**, 201 (2003).
- [28] H. Huang, X. Yang, M. Krafczyk, and X.-Y. Lu, Rotation of spheroidal particles in Couette flows, *J. Fluid Mech.* **692**, 369 (2012).
- [29] O. Aouane, A. Scagliarini, and J. Harting, Structure and rheology of suspensions of spherical strain-hardening capsules, *J. Fluid Mech.* **911**, A11 (2021).
- [30] v. H. Eilers, Die viskosität von emulsionen hochviskoser stoffe als funktion der konzentration, *Kolloid-Z.* **97**, 313 (1941).
- [31] D. Chappell, J. Stapley, B. Rashid, M. Towns, W. J. Andrews, M. Kiani, and M. Salehi, Successful field trial of a shear-resistant, high-injectivity, reservoir-triggered polymer, in *Abu Dhabi International Petroleum Exhibition & Conference, Abu Dhabi, UAE* (OnePetro, USA, 2017), Paper No. SPE-188528-MS.